Drift of scroll waves of electrical excitation in an isotropic model of the cardiac left ventricle

S. F. Pravdin[*], H. Dierckx[†], and A. V. Panfilov[†]

Abstract — The dynamics of scroll waves in a symmetric isotropic model of the human cardiac left ventricle is considered. The position of the attractor and the wave rotation velocity over the attractor were determined depending on the wall thickness, parameters of the cell model, chirality of the wave, and the initial position. Mechanisms of observed phenomena are discussed.

One of the most important spatial dynamic regimes in excitable media are spiral waves rotating around a domain called the core, which contains a phase singularity [32,36]. The spiral waves in the three-dimensional media are called scroll waves. They were found in oscillating chemical reactions [16] and in living systems [35], for example, in populations of Dictyostelium discoideum amoebae [19], on the retina [14], in xenopus oocytes [18]. Scroll waves in the myocardium [6] are associated with dangerous cardiac arrhythmias [2,7]. It is important to understand what factors affect the dynamics of scroll waves in the heart, as they determine the type of arrhythmias [12]. For example, as was shown, the drift of scroll waves underlies the polymorphic ventricular tachycardia [13].

The drift of scroll waves may be caused by several reasons, in particular, by the anisotropy of the medium and the geometry of the domain where the wave rotates. For two-dimensional spiral waves it was shown in [8] that the wave drifts on anisotropic surfaces under a certain angle to the gradient of the intrinsic curvature of the surface.

In the three-dimensional case, there are other purely spatial effects that play an important role in the dynamics of scroll waves in the heart. In particular, it was shown that the wave drifts if its filament (the line around which the wave rotates) is

curved, and there exist different modes of such drift [23]. Depending on parameters, the length of the curved filament may decrease, and we assume here that its tension is positive as for a usual elastic body. If the filament elongates, then its tension is negative [4]. Such dynamics of filaments has an important value because it may lead to turbulence [17]. It was also shown in the theory that the drift of a filament is essentially affected by its shape [22]. However, until now the drift of filaments was usually studied on the models of simple geometry.

An anatomic model of the human cardiac left ventricle (LV) was developed in the Ural Branch of the Russian Academy of Sciences (UB RAS). This model correctly describes the form and direction of muscle fibres in LV [27]. It was constructed analytically and allows one to continuously change the shape and anisotropy of LV. Using this model, we can study the influence of the form and thickness of the myocardial wall on different types of cardiac arrhythmias.

Computational cardiology uses now two types of electrophysiological models, namely, simplified models describing only general properties of the cardiac tissue and detailed ones describing the biophysical mechanism of cardiac cells excitation. The use of models of one or other type depends on various factors, i.e., computational cost, availability of information on the studied object, problems to be solved [21]. It is important to know how the results obtained from different models correspond to each other. In this regard, in this paper we compare the dynamics of scroll waves of the electric excitation in the isotropic model of the human cardiac left ventricle for the simplified cardiomyocyte AP model of Aliev–Panfilov [1] and the biophysical TP06 model of ten Tusscher–Panfilov [33].

The aim of this paper is to compare the dynamics of a scroll wave filament based on those two cell models and also a numerical study of the influence of the filament tension, the chirality of wave rotation, and the ratio of the LV wall thicknesses at the base and at the apex of the ventricle on the drift of the filament.

1. Models and methods

The simulations of the electrophysiological activity of LV were performed based on two following cell models: the dimensionless phenomenological AP model [1] and the biophysical TP06 model of cells of the working ventricular myocardium of the human heart [33]. In order to calculate the propagation of excitation waves in the tissue, we used the mono-domain reaction–diffusion equations describing a homogeneous isotropic medium having the following general from:

$$\frac{\partial u}{\partial t} = D\Delta u + f(u, \mathbf{v})$$

$$\frac{\partial \mathbf{v}}{\partial t} = \mathbf{g}(u, \mathbf{v})$$

where $u = u(\mathbf{r}, t)$ is the transmembrane cell potential at the point $\mathbf{r}$ at the time moment t, D is the diffusion coefficient, $\mathbf{v}$ is the vector of other phase variables of the model, $f(u, \mathbf{v})$ and $\mathbf{g}(u, \mathbf{v})$ are functions dependent on the cardiomyocyte model.

In the case of the AP model the system has the form

$$\frac{\partial u}{\partial t} = D\Delta u - ku(u-a)(u-1) - uv$$

$$\frac{\partial v}{\partial t} = \varepsilon(u)(ku - v)$$

where

$$\varepsilon(u) = \begin{cases} 1, & u < a \\ 0.1, & \text{otherwise.} \end{cases}$$

The TP06 model has the following general form:

$$\frac{\partial u}{\partial t} = D\Delta u - \frac{I_{\text{ion}}}{C_{\text{m}}}$$

$$I_{\text{ion}} = I_{Kr} + I_{Ks} + I_{K1} + I_{to} + I_{\text{Na}} + I_{b\text{Na}} + I_{\text{CaL}} + I_{b\text{Ca}} + I_{\text{NaK}} + I_{\text{NaCa}} + I_{p\text{Ca}} + I_{pK}.$$

Intracellular processes are described here by a sum of ion currents $I_{\text{ion}} = I_{\text{ion}}(\mathbf{r}, t)$; C_{m} is the capacity of the cellular membrane (see [33] for details).

The dynamics of a spiral wave is often represented by the following approach. At some isoline of the transmembrane potential the point of 'tip' of a spiral wave is determined as the point of transition of the wave front to the wave back. (In fact, if we follow the isoline, then we move from points of the front to points of the back and hence there is a transition point between them.) As was shown in [11], this point $\mathbf{r}_{\text{tip}}$ can be approximated by the following system of equations:

$$u(\mathbf{r}_{\text{tip}}, t) = u^*$$

$$u(\mathbf{r}_{\text{tip}}, t + \Delta t) = u^*$$

where the values u^* and Δt are chosen differently for each model. In our case these values were $u^* = -60$ mV for the TP06 model, $u^* = 0.5$ for AP model; $\Delta t = 8$ ms in the TP06 model, and in the AP model the value of Δt was equal to $T = 17$ ms. Analyzing the trajectory of this point, one can determine the mean drift velocity of the spiral wave and the type of its dynamics.

A scroll wave rotates around some curve called *filament*. Dividing the myocardium into layers, we can obtain the filament from the nodes being centers of rotation of spiral waves in each separate layer. The *tension* of the filament characterizes the tendency of the scroll wave to break up. We calculated the tension using the methodology from [20, 23, 24], i.e., we solved the system

$$\frac{\partial u}{\partial t} = D\Delta u + f(u, \mathbf{v}) + \frac{D}{R} \cdot \frac{\partial u}{\partial x}$$

$$\frac{\partial \mathbf{v}}{\partial t} = \mathbf{g}(u, \mathbf{v})$$

Table 1.
Tension of the filament.

Model	Tension, mm^2/ms
AP:	
$a = 0.03$	1.2
$a = 0.065$	0.13
$a = 0.08$	-2
TP06	0.6

in the square $x \in [0, N\Delta r]$, $y \in [0, N\Delta r]$, $t \in [0, T]$, $N = 600$, $\Delta r = 0.4$, for $D = 1$ and the radius of the vortex ring filament $R = 10$ (see details in [24]) with initial conditions providing the appearance of a spiral wave and for sufficiently large T. We determined the center of rotation $\mathbf{r}_{\text{tip}}(t)$ of the spiral wave and decomposed it in a sum of a periodic function (rotation) and a linear function (drift), i.e.,

$$\mathbf{r}_{\text{tip}}(t) = \mathbf{r}_{\text{tip}}^{\text{per}}(t) + \mathbf{v}^{\text{drift}}t$$

where $\mathbf{v}^{\text{drift}} = (v_x^{\text{drift}}, v_y^{\text{drift}})$. The tension b_2 (notation from [5]) was calculated by the formula

$$b_2 = -v_x^{\text{drift}} R.$$

The values of parameter of the ionic model were taken from [33]; these values correspond to physiological characteristics of cardiomyocytes. The diffusion coefficient was $D = 0.154$ mm^2/ms. For the AP model the parameters were the following: the diffusion coefficient $D = 12$, $k = 8$, $a \in \{0.03, 0.065, 0.08\}$. The different values of the parameter a were considered to obtain the different values of filament tension. We calculated the tension for all models used in our calculations (Table 1).

For comparison of the results, the values obtained in the AP and TP06 models must be represented in the same units. In the TP06 model the units are mm and ms. Using the method from [1, 21] and comparing the period and wavelength of the spiral wave in the TP06 and AP models, we found that the time unit in the AP model is 17 ms and the space unit is 8.4 mm.

The LV had an axially symmetric form described in [27] and the following parameters: the outer (epicardial) radius $R_b = 33$ mm on the base, the thickness $L = 12$ mm on the base, the height $Z_b = 60$ mm, and the coefficient of ellipticity $\varepsilon = 0.85$. In different experiments we varied the thickness of the LV at the apex making it thinner or thicker than the base, i.e., $h = 6, 8, \ldots, 18$ mm.

In the AP model the time step was $dt = 1.666 \cdot 10^{-3} \, T \approx 0.03$ ms, the spatial step was $dr = 0.8$ mm. In the TP06 model we had $dt = 0.02$ ms and $dr = 0.28$ mm.

We used no-flux boundary conditions. The LV geometry is constructed using a special coordinate system (γ, ψ, φ) similar to a spherical one. Its coordinate γ is responsible for the layer of the wall from the endocardium $\gamma = 0$ to the epicardium $\gamma = 1$; ψ corresponds to the position of a point relative to the base $\psi = 0$ and apex $\psi = \pi/2$ of the ventricle; the angle $\varphi \in [0, 2\pi)$ is an analogue of longitude. In this coordinate system we constructed a grid that is uniform in special coordinates

Table 2.
Position of the thinnest part of the wall in LV model.

h, mm	ψ_0	ψ_1	d^*, mm
	1.571	1.571	6.0
6			
	1.354	1.412	7.96
8			
10	1.097	1.205	9.51
12	0.878	1.001	10.621
14	0.645	0.756	11.349
16	0.389	0.463	11.731
18	0.198	0.234	11.876

and non-uniform in the Cartesian ones. Grid nodes have the indices in γ, ψ, φ from 0 to $N_\gamma = 12$, $N_\psi = 93$, $N_\varphi = 255$, respectively (the algorithm was described in [28]). After adjustment, the distance between nodes was 0.8 mm in average (from 0.3 to 1.36 mm). The use of special coordinates makes it easier to represent the boundary condition in contrast to uniform grids in the Cartesian coordinates where the representation of the boundary condition may cause some difficulties.

When studying the dynamics of filaments in a domain of variable thickness, it is important to know where the thinnest part of the body is located. In this case we determined the thinnest part of the LV wall solving the following extremum problem:

$$d(\psi_0, \psi_1) = |\mathbf{r}(0, \psi_0) - \mathbf{r}(1, \psi_1)| \xrightarrow[\psi_0, \psi_1]{} \min$$

where $\mathbf{r}(\gamma, \psi)$ is the radius vector of a point in LV with the special coordinates γ, ψ, $\varphi = 0$; $0 \leqslant \psi_{0,1} \leqslant \pi/2$. The results are presented in Table 2 (d^* is the minimal thickness of the wall) and in Fig. 1.

The LV model used here allows us to change its geometrical parameters easily, for example, to change the ratio of the wall thickness at the apex and on the base. This ratio is important in the study of the drift of spiral waves, which, according to the theory of spiral waves, goes in the direction of the wall thinning for a positive tension of the filament.

In order to create a spiral wave, we used the temporary block of excitation in the AP model and the S1S2 protocol in the TP06 model.

The AP model used two following protocols of initial stimulation: 'psi4' and 'psi8' (initial increase of the potential $u = 1$ at the nodes with the indices from 0 to N_γ for γ, from 0 to $0.4N_\psi$ or $0.8N_\psi$ for ψ, and from 0 to 29 for φ; increased value $v = 1$ at the nodes with the indices from 0 to N_γ for γ, from 0 to $0.4N_\psi$ or $0.8N_\psi$ for ψ, and from 30 to 60 for φ). In this case the filament appears on the latitude of approximately 40% and 80% of the maximal one, respectively.

Protocol S1S2 (chirality 1) assumed the initial stimulation ($u = 0$ mV) in the domain $x \in [126, 140]$, $y \in [130, 250]$, $z \in [150, 250]$, and sensed the potential at the point $A(126, 193, 114)$. The second stimulus in the domain $x \in [134, 250]$, $y \in [0, 250]$, $z \in [100, 250]$ at the moment when the potential at the point A becomes
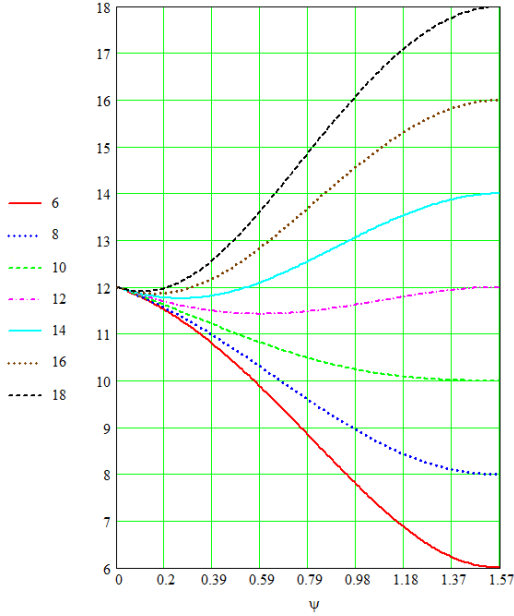
Figure 1. Dependence of the wall thickness (in mm) in the LV model on the latitude ψ. Different lines correspond to different thickness of the ventricular wall at the apex (h, mm, see the legend). The base of the ventricle has the latitude $\psi = 0$, the apex has the latitude $\psi = \pi/2$.

less than -82 mV after it raised greater than -40 mV. For the case of chirality 2 the stimulation used the following parameters: the initial stimulation in the same domain, the control of the same point, the second stimulus in the domain $x \in [0, 114]$, $y \in [0, 250]$, $z \in [100, 250]$. The coordinates are indicated in a cube with the side of 250 where LV was placed. The epicardium apex had the coordinates (125, 125, 18) in the cube.

To simplify the study of the filament dynamics, we considered the trajectory of the middle point of the filament. The movement of this midpoint consists of two components, namely, relatively fast rotation around the core and a slower drift along a certain curve. We averaged the trajectories of the filament midpoint in the special coordinates (ψ, φ) over $N = 2$ periods of rotation around the core. To do that, we calculated the phase angle β in the plane (ψ, φ) at the moment i as $\beta_i = \arctan((\psi_{i+1} - \psi_i)/(\varphi_{i+1} - \varphi_i))$. In order the function $\beta(t)$ not to have jumps by $n\pi$, $n \in \mathbb{Z}$, we added the corresponding terms $n\pi$ to it. The result $(\psi_{av,i}, \varphi_{av,i})$ yielded the mean coordinates (ψ, φ) between the phases $\beta_i - 2\pi$ and $\beta_i + 2\pi$.

We studied the filament dynamics depending on its tension, direction of rotation (chirality), the LV wall thickness at the apex with a constant thickness at the base, and for simplified and detailed cell models.

The calculations for the AP model were performed using the software [31] developed by our team from Institute of Mathematics and Mechanics of the UB RAS on the cluster 'URAN' of the UB RAS. For parallel calculations on multiple cores of one computing node we used OpenMP technology. The code used the Intel C

compiler 'icc'. The numerical algorithm utilized a grid method based on explicit Euler's method.

The calculations for the ionic model were performed by the software developed in Ghent University using the CUDA technology on clusters of the UB RAS ('URAN') and Ural Federal University. The software used the Nvidia C compiler 'nvcc'. Computational nodes were equipped with graphical processors Tesla K40m0.

2. Results

In the following computational experiments we varied the LV wall thickness, chirality, and the initial position of the filament.

In our LV model the drift of the filament midpoint averaged over the period consisted of two phases [28]. In the first phase the filament drifts from the initial position to the attractor and also rotates around the axis of LV. In the second phase the coordinate ψ stabilizes and the scroll wave drifts around the axis of LV with another speed which was often greater than the speed in the first phase. Note that in the second drift phase the trajectory of the filament after its averaging over the period and thickness of the LV wall approaches a circle lying in a plane orthogonal to the LV axis. The position of that circle and the linear speed of filament drift over it were chosen as measured characteristics.

Examples of the filament midpoint trajectories are presented in Fig. 2. We see that for a negative tension the core of the vortex is larger than for a positive tension.

The duration of the transition process, i.e., the drift of filament from its origin to the attractor is presented for a positive tension in Fig. 3. We see that in the AP model the greater the difference in thickness between the apex and the base is, the shorter this time is. In the ionic model such dependence is not observed, and the time generally increases with the growth of the thickness of the apex.

All the results presented below relate to the middle point of the filament after averaging its trajectory over the period, i.e., we neglect the variations of the length and form of the filament and also the rotation around the core.

The trajectories of filament midpoints for a positive tension are presented in Fig. 4. In the cases of thin and thick apex ($h = 6$, 18 mm) the meridional drift of the wave is presented in AP model, but is absent or relatively small in the TP06 model. Other results were obtained for equal thicknesses of the apex and base ($h = 12$ mm). For both models the wave practically does not drift around the axis of the ventricle. In one case of those six, for $h = 6$ mm in the ionic model, the longitudinal direction (in φ) of the drift was changed by an opposite one at the end of the first phase. Graph B also shows that the time needed to reach the attractor is several times less in the AP model than in the TP06 model.

The graphs of the coordinate ψ of the filament midpoint attractor are presented in Fig. 5 depending on the model, initial conditions (i.e., the position of filament origin), chirality, and the filament tension.

First we analyze the dependence on the filament initial position (variants 'psi4'
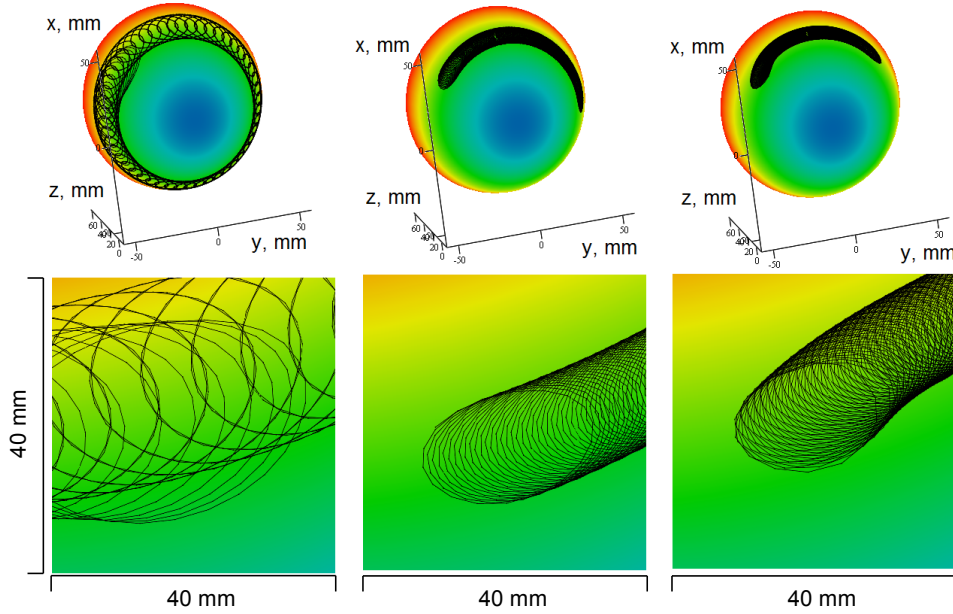
Figure 2. Filament midpoint trajectory in the model of Aliev–Panfilov, the stimulation is 'psi4'. Top row: bottom view to the LV model as a whole, bottom row: zone of filament origin for the initial stimulation, zoomed 4 times. Left column: $a = 0.08$, middle column: $a = 0.065$, right column: $a = 0.03$. The wall thickness at the apex is 16 mm.

and 'psi8'). We see that there is no dependence for the AP model with a positive tension (lilac and purple lines for $a = 0.03$ coincide in Fig. 5A). On the other hand, for the AP model with a negative tension (Fig. 5B) there is almost no displacement of the filament in latitude from the position of its origin.

The analysis of cases with different chirality of waves in the ionic TP06 model shows that there is no dependence of ψ on the chirality of the vortex (solid and dotted black lines practically coincide in Fig. 5A). It should be noted that the chirality 1 corresponds to the clockwise rotation (if we look at LV from the epicardium of the apex) and the chirality 2 corresponds to the counterclockwise rotation.

If the thickness h of the LV wall at the apex changes, then the attractor also changes its position for nonnegative filament tension in both models. For $h < 12$ mm we have a thinner LV wall near the apex and the filament moves to the apical region of the ventricle ($\psi > \pi/4$). If $h > 12$ mm, then the thinner wall is near the LV base and the filament drifts to the base ($\psi < \pi/4$).

The graph of the speed of filament rotation around the axis of LV is presented in Fig. 6. We have seen that the speeds differ by 2 orders of magnitude and hence we used different OY axes, namely, from -1 to $+1.25$ mm/s for the TP06 model and for AP model with the parameters $a = 0.03$ and 0.065 (Fig. 6A) and from -0.02 to $+0.015$ mm/s for the remaining case, i.e., the AP model with $a = 0.08$ (Fig. 6B).

The graphs show that the speed in the AP model does not depend on the position of filament origin for a positive tension (lilac and purple lines for $a = 0.03$ coincide
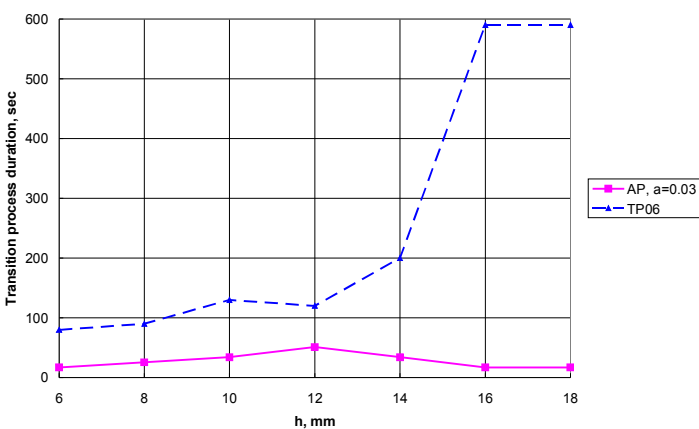
Figure 3. Duration of the transition process (seconds) depending on the cell model and thickness of LV at the apex.

in Fig. 6A), but depends on it for a negative tension (blue and light blue lines do not coincide in Fig. 6B).

Concerning the dependence of the speed on the tension itself, this dependence is seen very clearly, for a positive tension (lilac and purple lines for $a = 0.03$ in Fig. 6A) the speed has the order in magnitude up to tenth of mm/s, and for positive values (Fig. 6B) up to hundredths of mm/s.

If the rotation changes its direction, the drift speed is reversed staying the same in the absolute value (see Fig. 6A).

3. Discussion

3.1. Position of the filament attractor

The results obtained here related to the position of the filament attractor (see Fig. 5) can be explained by using the notion of filament tension b_2 [5, 34], see Table 1.

The filament shortens in the AP model with $a = 0.03$ and in the ionic model. Based on this information, we can explain the graphs presented in Fig. 5A as a drift in the direction of minimal thickness of ventricular wall, i.e., if the apex thickness increases, the position of the minimal thickness of ventricular wall gradually moves from the apex to the base ($\psi \to 0$).

It is interesting that for the AP and TP06 models we get tensions of the same order, although the models are completely different. In particular, the form of the action potential essentially differs in these two models, especially in the duration (width) of the wave front of excitation.

In the case of negative filament tension ($a = 0.08$ in AP model, see Fig. 5B) we see a qualitatively different picture; the filament elongates, which, as is known, can cause a break up and turbulence of the vortex above a sufficient thickness of the medium [5, 23, 25]. However, if the thickness of the medium is comparable to
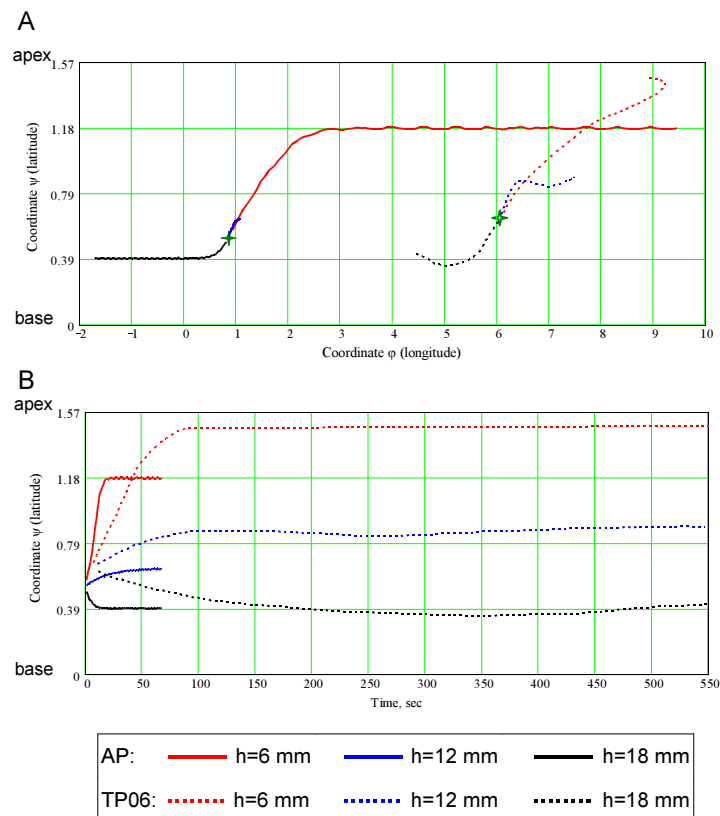
Figure 4. The trajectories of filament midpoints after averaging over the period for model of myocardium cells with positive tension: AP model, $a = 0.03$, and ionic TP06 model. Three models of a ventricle. Green 'cross' indicates the origin of the filament (solid figure for AP model, without filling for TP06 model).

the radius of the vortex core or even less than it, the rigidity of the filament [3, 10] prevents the appearance of complete spatial instability and can lead to a bending of the filament. In our experiments the filament was slightly curved and depending on the initial conditions it stayed approximately at the same latitude where it originates either near the apex (for 'psi8' initial conditions) or near the base (for 'psi4').

3.2. Speed of the filament drift at the attractor

The curvature of the filament causes its drift in the plane perpendicular to the filament. This drift is proportional to the filament curvature k and has two components, i.e., along the normal N and along the binormal B of the filament. The drift coefficient along the normal (b_2 in [5, p. 617]) is also called the scalar component as it does not depend on the chirality of the vortex. The coefficient in binormal direction (c_3) is called the pseudoscalar component as it changes its sign with changing the

A

B
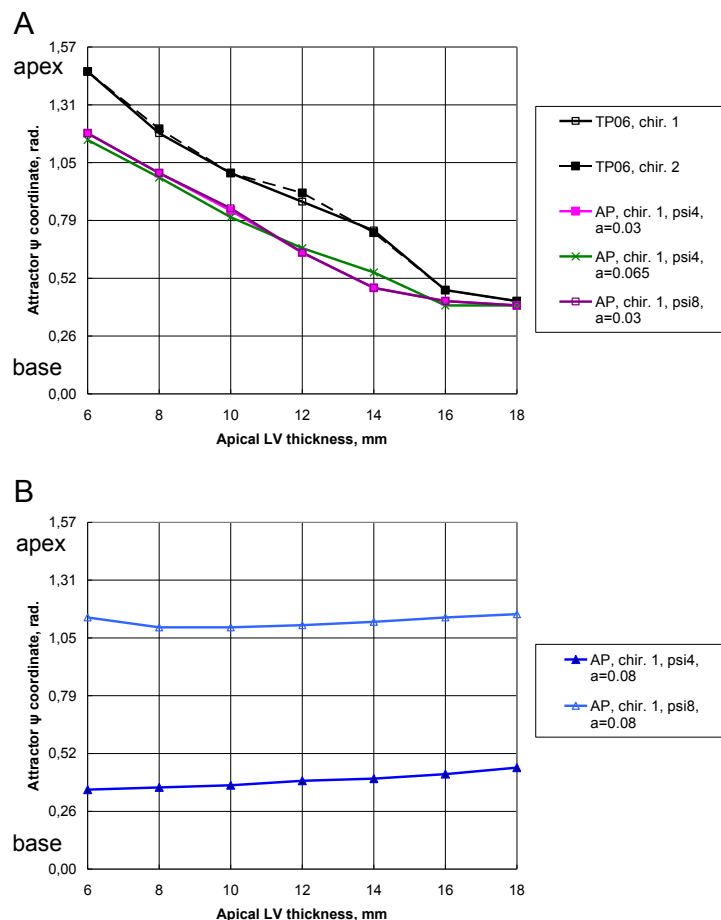
Figure 5. Position of the filament in the LV wall of irregular thickness. A is the case of positive filament tension, B is the case of negative tension.

chirality of the vortex.

In our calculations, if we neglect the rotation of the filament around the core, the attractor is a circle at a constant latitude ψ, i.e., a parallel of LV. The reason is that the gradient of any parameter causing the drift of the filament (those can be the gradient of the wall thickness, of some parameter of the cell model [26], of the wall curvature [8], etc.) leads to appearance of a scalar drift component along or against the gradient and a pseudoscalar component in the normal direction to the gradient (see more examples in [8]). The pseudoscalar component changes its sign with the change of the chirality. We use an axially symmetric LV model and hence all geometric gradients (the thickness and curvature of the ventricular wall) have the meridional direction, and the position of the attractor is determined by the equilibrium of scalar drift components. However, scalar and pseudoscalar coefficients in one or other model are, generally speaking, different, and as the result we see a
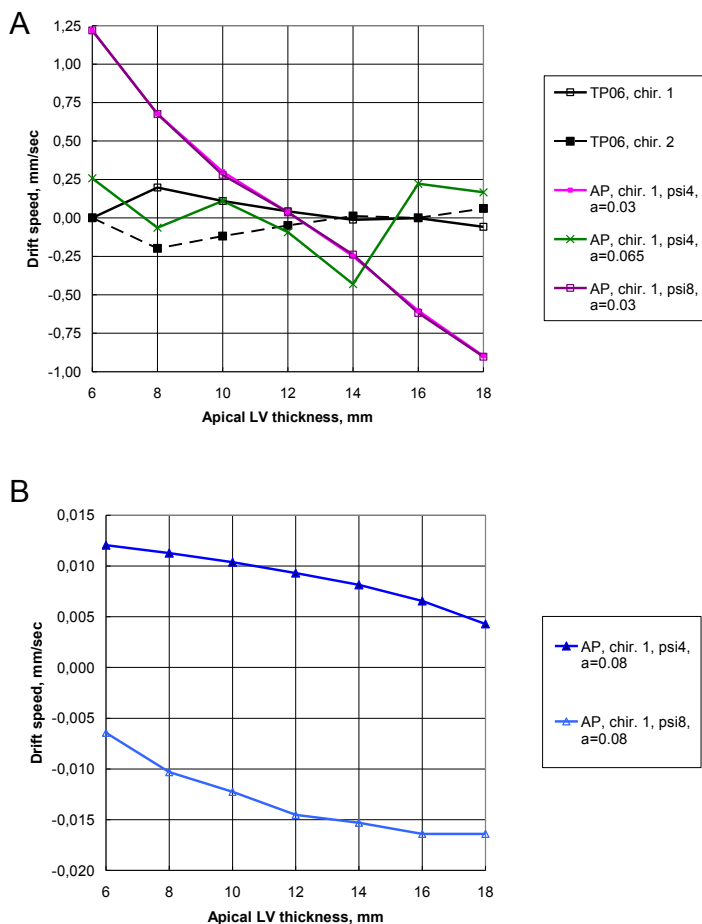
Figure 6. Linear speed of the filament rotation around the attractor: A is the case of the positive filament tension, B is the case of the negative tension.

remaining pseudoscalar drift along parallels, i.e., around LV (circular drift).

The results of calculations on the ionic models (Fig. 6A) clearly show that the circular drift goes in the opposite direction when changing the chirality of the scroll wave. For the apical thickness $h > 8$ mm the circular speed of the drift depends monotonically on h.

In the case of small tension ($a = 0.065$, the green line in Fig. 6A) there are some difficulties for analysis; apparently, this complicated behaviour of the system is caused by the mutual influence of different geometrical factors of higher orders (see, e.g., [9]).

Considering the last case, i.e., the AP model with a negative tension ($a = 0.08$, see Fig. 6A), we can indicate that the drift speed is smaller, for example, for $h = 6$ mm the speed is $v = 0.012$ mm/s for $a = 0.08$ and $v = 0.258$ mm/s for $a = 0.065$. This is typical for a curved filament because the largest component of the

pseudoscalar drift (c_3 in [5], γ_2 in [34]) causes the precession of the filament [10]. Due to this fact, the displacement of the filament can be caused by only terms of higher orders [9], which leads to significant drop in speed compared to the straight filament.

The tension in the TP06 model is 2 times less than in the AP model for $a = 0.03$, but the ratio of drift speeds, as is seen from Fig. 6A, depends on the wall thickness h at the apex only. This indicates that not only the tension, but other differences of the models play their role. For example, in the ionic model the ratio of the front length to the action potential duration is much greater than in the AP model. This may be one of the reasons for the differences. However, this problem requires further study.

The results concerning the drift of filaments in the AP model were presented in [29] for the cases of isotropy and anisotropy in a similar model of LV. It should be noted that drift speeds in [29] and in the present paper differ due to different scaling of units.

4. Conclusions

We have studied the drift of excitation waves in a symmetric isotropic model of the human cardiac left ventricle. The calculations show that for both used models of cardiomyocytes the position of the filament attractor similarly depends on the thickness of the LV wall for a positive tension, but there are essential quantitative differences. Qualitatively different results were obtained for the speed of the filament rotation in these two models. Further investigations will be focused on detailed studies of the wave drift in an anisotropic model of the ventricle.

Acknowledgements

References

1. R. R. Aliev and A. V. Panfilov, A simple two-variable model of cardiac excitation. *Chaos, Solitons and Fractals* **7** (1996), No. 3, 293–301.

2. M. A. Allessie, F. I. M. Bonke, and F. J. G. Schopman, Circus movement in rabbit atrial muscle as a mechanism of tachycardia, III. The 'leading circle' concept: a new model of circus movement in cardiac tissue without the involvement of an anatomical obstacle. *Circulation Research* **41** (1977), No. 1, 9–18.

3. S. Alonso and A. V. Panfilov, Negative filament tension in the Luo–Rudy model of cardiac tissue. *Chaos* **17** (2007), 015102/1–015102/9.

4. S. Alonso, F. Sagues, and A. S. Mikhailov, Taming winfree turbulence of scroll waves in excitable media. *Science* **299** (2003), No. 5613, 1722–1725.

5. V. N. Biktashev, A. V. Holden, and H. Zhang, Tension of organizing filaments of scroll waves. *Philos. Trans. Royal Soc. London, Ser. A: Math. Phys. Sci. Engrg.* **347** (1994), No. 1685, 611–630.

6. E. M. Cherry and F. H. Fenton, Visualization of spiral and scroll waves in simulated and experimental cardiac tissue. *New J. Phys.* **10** (2008), 125016.

7. J. M. Davidenko, A. V. Pertsov, R. Salomonsz, W. Baxter, and J. Jalife, Stationary and drifting spiral waves of excitation in isolated cardiac muscle. *Nature* **355** (1992), No. 6358, 349–351.

8. H. Dierckx, E. Brisard, H. Verschelde, and A. V. Panfilov, Drift laws for spiral waves on curved anisotropic surfaces. *Phys. Rev. E: Stat., Nonlinear, and SoP Matter Phys.* **88** (2013), No. 1, 012908.

9. H. Dierckx and H. Verschelde, Effective dynamics of twisted and curved scroll waves using virtual filaments. *Phys. Rev. E* **88** (2013), No. 6, 062907.

10. H. Dierckx, H. Verschelde, Ö. Selsil, and V. N. Biktashev, Buckling of scroll waves. *Phys. Rev. Lett.* **109** (2012), No. 17, 174102.

11. F. H. Fenton and A. Karma, Vortex dynamics in three-dimensional continuous myocardium with fiber rotation: filament instability and fibrillation. *Chaos* **8** (1998), No. 1, 20–47.

12. A. Garfinkel, P.-S. Chen, D. O. Walter, H. S. Karagueuzian, B. Kogan, S. J. Evans, M. Karpoukhin, C. Hwang, T. Uchida, M. Gotoh, O. Nwasokwa, P. Sager, and J. N. Weiss, Quasiperiodicity and chaos in cardiac fibrillation. *J. Clinical Invest.* **99** (1997), No. 2, 305–314.

13. A. Garfinkel and Z. Qu, Nonlinear dynamics of excitation and propagation in cardiac tissue. In: *Cardiac Electrophysiology: From Cell to Bedside* (Eds. D. P. Zipes and J. Jalife). Saunders, Philadelphia, USA, 2000, pp. 315–320.

14. N. A. Gorelova and J. J. Bures, Spiral waves of spreading depression in the isolated chicken retina. *J. Neurobiol.* **14** (1983), No. 5, 353–363.

15. R. Imbihl and G. Ertl, Oscillatory kinetics in heterogeneous catalysis. *Chem. Rev.* **95** (1995), No. 3, 697–733.

16. R. Kapral and K. Showalter (eds.), *Chemical waves and patterns*. In: *Understanding chemical reactivity*. Vol. 10. Springer-Science, Kluwer Acad. Publ., Dordrecht, 1995.

17. J. P. Keener, The dynamics of three-dimensional scroll waves in excitable media. *Physica D. Nonlinear Phenomena* **31** (1988), No. 2, 269–276.

18. J. Lechleiter, S. Girard, E. Peralta, and D. Clapham, Spiral calcium wave propagation and annihilation in Xenapus laevis oocytes. *Science* **252** (1991), No. 5002, 123–126.

19. K. J. Lee, R. E. Goldstein, and E. C. Cox, Resetting wave forms in Dictyostelium territories. *Phys. Rev. Lett.* **87** (2001) No. 6, 068101.

20. A. V. Panfilov, R. R. Aliev, and A. V. Mushinsky, An integral invariant for scroll rings in a reaction–diffusion system. *Phys. D* **36** (1989), 181–188.

21. A. V. Panfilov and A. V. Holden, Computer simulation of re-entry sources in myocardium in two and three dimensions. *J. Theor. Biol.* **161** (1993), 271–285.

22. A. V. Panfilov and J. P. Keener, Re-entry in three-dimensional Fitzhugh–Nagumo medium with rotational anisotropy. *Phys. D. Nonlinear Phenom.* **84** (1995), No. 3–4, 545–552.

23. A. V. Panfilov and A. N. Rudenko, Two regimes of the scroll ring drift in the three-dimensional active media. *Phys. D. Nonlinear Phenom.* **28** (1987), No. 1–2, 215–218.

24. A. V. Panfilov, A. N. Rudenko, and V. I. Krinsky, Scroll rings in three-dimensional active medium with two component diffusion. *Biofizika* **31** (1986), 850–854.

25. A. V. Panfilov and B.N. Vasiev, Vortex initiation in a heterogeneous excitable medium. *Physica D* **49** (1991), 107–113.

26. A. M. Pertsov and E. A. Ermakova, Mechanism of the drift of a spiral wave in an inhomogeneous medium. *Biofizika* **33** (1988), No. 2, 338–342.

27. S. F. Pravdin, V. I. Berdyshev, A. V. Panfilov, L. B. Katsnelson, O. Solovyova, and V. S. Markhasin, Mathematical model of the anatomy and fibre orientation field of the left ventricle of the heart. *Biomed. Engrg. Online* **12** (2013), No. 54, 21.

28. S. F. Pravdin, H. Dierckx, L. B. Katsnelson, O. Solovyova, V. S. Markhasin, and A. V. Panfilov, Electrical wave propagation in an anisotropic model of the left ventricle based on analytical description of cardiac architecture. *PLoS ONE* **9** (2014), No. 6, e93617.

29. S. F. Pravdin, H. Dierckx, V. S. Markhasin, and A. V. Panfilov, Drift of scroll wave filaments in an anisotropic model of the left ventricle of the human heart. *Biomed. Res. Int.* **2015** (2015), 389830.

30. S. Sinha and S. Sridhar, *Patterns in Excitable Media. Genesis, Dynamics, and Control*. CRC Press, 2015.

31. A. Sozykin, S. Pravdin, A. Koshelev, V. Zverev, K. Ushenin, and O. Solovyova, LeVen — a parallel system for simulation of the heart left ventricle. In: *Proc. 9th Int. Conf. on Application of Information and Communication Technologies (AICT)* (Ed. A. Adamov). 2015, pp. 249–252.

32. K. H. W. J. ten Tusscher, A. Mourad, M. P. Nash, R. H. Clayton, C. P. Bradley, D. J. Paterson, R. Hren, M. Hayward, A. V. Panfilov, and P. Taggart, Organization of ventricular fibrillation in the human heart: experiments and models. *Exp. Physiol.* **94** (2009), No. 5, 553–562.

33. K. H. ten Tusscher and A. V. Panfilov, Alternans and spiral breakup in a human ventricular tissue model. *Amer. J. Physiol. Heart Circ. Physiol.* **291** (2006), No. 3, H1088-100.

34. H. Verschelde, H. Dierckx, and O. Bernus, Covariant stringlike dynamics of scroll wave filaments in anisotropic cardiac tissue. *Phys. Rev. Lett.* **99** (2007), No. 16, 168104.

35. *Self-Organized Biological Dynamics and Nonlinear Control* (Ed. J. Walleczek). Cambridge Univ. Press, 2000.

36. A. T. Winfree and S. H. Strogatz, Organizing centres for three-dimensional chemical waves. *Nature* **311** (1984), 611–615.